Electronics and Communications in Japan, Part 2, Vol. 77, No. 7, 1994
Translated from Denshi Joho Tsushin Gakkai Ronbunshi, Vol. 77-C-II, No. 3, March 1994, pp. 148-159

Picture Quality of Different Pixel Arrangements for Large-Sized Matrix Displays

Zen-ichiro Hara and Nobuo Terazaki, *Nonmembers*

Nagasaki Works, Mitsubishi Electric Corporation, Nagasaki, Japan 852-91

Naoki Shiramatsu and Shuji Iwata, *Members*

Materials and Electronic Devices Laboratory, Mitsubishi Electric Corporation, Amagasaki, Japan 661

SUMMARY

The image information theory is introduced to the study of pixel arrangement for flat displays which has been based mainly on subjective evaluation tests. The objective is to make a theoretical elucidation of the relations between different pixel arrangements—particularly pixel arrangements of light-emissive elements for large-sized matrix displays—and picture quality.

First, the factors determining picture quality are identified using a picture model incorporating the sampling of the original picture. As a result, the Nyquist limits are shown to be essential.

Second, the Nyquist limits of different pixel arrangements are evaluated. The areas surrounded by the Nyquist limits are shown to consist of colored and discolored regions. This observation is used to relate the Nyquist limits to visual limits and picture quality.

Third, the picture quality of typical pixel arrangements for large-sized matrix displays is examined. The quality of still and motion pictures displayed by the RGB-trio and RGGB-mosaic arrangements are compared by means of subjective evaluation tests and three-dimensional spectrum analysis. The comparative analysis gives the following conclusions:

(1) In displaying still pictures, the RGGB-mosaic arrangement has the effective number of pixels about twice the real number of pixels because of the overlaps of adjacent pixels, but the RGB-trio does not have this effect.

(2) In displaying motion pictures, the RGGB-mosaic arrangement provides better picture quality than in the case of still pictures but the RGB-trio arrangement does not.

Key words: Large-sized matrix display; pixel arrangement; subjective evaluation test of picture quality; three-dimensional Nyquist limits.

1. Introduction

With the development of an information society, color displays based on arranged light-emissive elements (large-sized matrix displays) have been finding increasing use since they were put into practical use in 1980 [1].

ISSN8756-663X/94/0007-0105

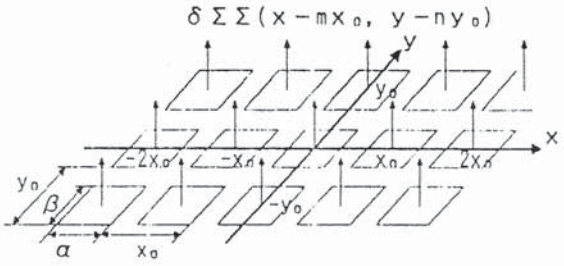

Fig. 1. Model of the flat display.

Over the years, these displays have been developed from the previous system based on single-pixel light-emissive elements [1, 2] to those based on multiple-pixel light-emissive elements [3], and even now new light-emissive elements are being presented in rapid order [4, 5].

In the development of large-sized matrix displays, the arrangement of pixels is an important technical factor determining the electrode structure of light-emissive elements. At the same time, it also is important as an economic factor, i.e., for the purpose of providing high picture quality with a small number of pixels.

The study of the relation between pixel arrangement and picture quality which has produced several reports on flat displays such as the LCD has been conducted mainly by subjective evaluation tests using simulation pictures [6-8]. Recent reports considered such subjects as an attempt to quantify resolution by calculating two-dimensional resolution [9], and the introduction of Nyquist limits [10]. However, these studies are insufficient from a theoretical viewpoint. On the other hand, the studies based on simulation pictures also have limitations. For example, simulation pictures cannot provide sufficient pixels and are limited to specific still pictures or patterns. Therefore, in the study of the relation between pixel arrangement and picture quality, it is difficult to use the results of subjective evaluation tests as the basis for objective description.

By introducing image information theory to the study of pixel arrangement, this paper aims at a theoretical elucidation of the relation between the pixel arrangement of light-emissive elements for large-sized matrix displays and the picture quality provided by these displays.

In section 2, a model is presented which incorporates picture sampling. Using this model, the factors determining picture quality are identified.

In section 3, the model is applied to color displays. It is shown that the Nyquist limits are the essential factor in characterizing the displayed picture and that their structures consist of two regions, i.e., one capable of colored display and the other where the picture is discolored but its shape can be recognized. Furthermore, the Nyquist limits are related to the human visual limits and picture quality to study the relation between different pixel arrangements and picture quality.

In section 4, the picture quality of typical pixel arrangements for large-sized matrix displays is examined. The quality of still and motion pictures provided by the RGB-trio and RGGB-mosaic are compared by means of subjective evaluation tests and three-dimensional spectrum analysis.

2. Picture Model and Picture Quality Factors

To elucidate the relation between pixel arrangement and picture quality theoretically, it is necessary to consider a generalized picture while taking into account the sampling of the original picture. In this paper, a picture model is developed to identify the factors that determine the picture quality.

2.1. Picture model

Let us assume that the picture is displayed on the display shown in Fig. 1. Because many light-emissive elements are arranged in large-sized matrix displays, individual pixels must be arranged with gaps in between. Here, x and y are the coordinates of the two-dimensional space where the picture exists, x_0 and y_0 are the pixel pitches, and α and β are the pixel lengths in the x and y directions. The image is displayed when the pixels emit light according to the sampled information. To sample the original picture, a picture model is derived as follows.

First, express the original picture and its Fourier transformation by the following equations:

$h(x, y)$: original picture (1)

$$F\{h(x, y)\} = H(\mu, \nu) \tag{2}$$

where μ and ν are the spatial frequencies in the x and y directions. The sampled picture can be expressed by the

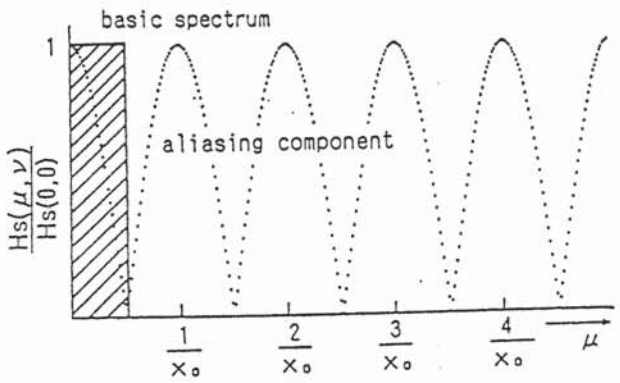

(a)

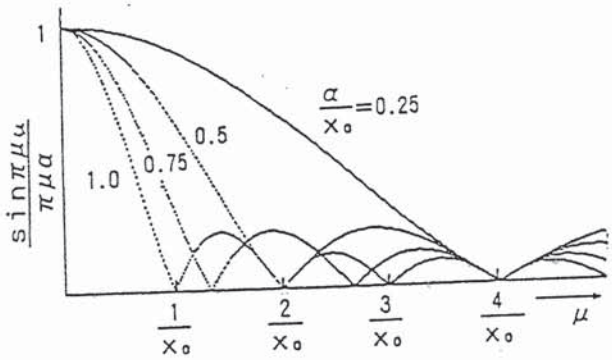

(b)

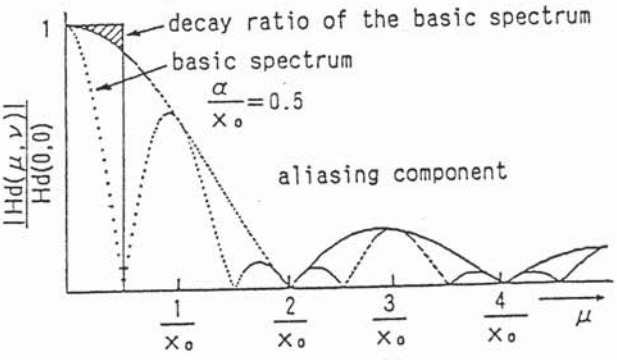

(c)

Fig. 2. (a) Relation between the basic spectrum and the aliasing component; (b) decay characteristics of the spectrum; and (c) spectrum of the picture.

product of the original picture and the sampling function [11]:

$$hs(x, y) = h(x, y) \cdot \sum_m \sum_n \delta(x - mx_0, y - ny_0) \qquad (3)$$

By performing Fourier transformation, we have [11]:

$$Hs(\mu, \nu) = \frac{1}{x_0 y_0} \sum_k \sum_l H\left(\mu - \frac{k}{x_0}, \nu - \frac{l}{y_0}\right) \qquad (4)$$

Equation (3) represents a picture shown on a display which arranges point pixels having a minute area. Thus, the picture on the flat display is expressed by the sum of Eq. (3) over the pixel area:

$$hd = \sum_u \sum_v hs(x - \alpha_u, y - \beta_v) \qquad (5)$$

where α_u and β_v represent any position within the pixel. By performing the Fourier transformation of Eq. (5) and replacing the summation by integration, we obtain the following:

$$Hd = \int_{-\beta/2}^{\beta/2} \int_{-\alpha/2}^{\alpha/2} Hs(\mu, \nu) \cdot \exp(-2\pi\mu x) \cdot \exp(-2\pi\nu y)\, dx\, dy \qquad (6)$$

If the emission from the pixel is uniform over the pixel area, $H_s(\mu, \nu)$ is constant in the range of the integration. Thus, it is possible to integrate Eq. (6); and we arrive at the following equation, the expression of the model of the picture shown on the flat display:

$$Hd(\mu, \nu) = \alpha\beta Hs(\mu, \nu) \frac{\sin\pi\mu\alpha}{\pi\mu\alpha} \cdot \frac{\sin\pi\nu\beta}{\pi\nu\beta} \qquad (7)$$

The interpretation of Eq. (7) is provided in the following section.

2.2. Picture quality factors of the flat display

The picture quality depends on the difference in recognition between the original picture $H(\mu, \nu)$ and its displayed picture $H_d(\mu, \nu)$, and it is accounted for on the basis of the interpretation of Eq. (7). Since Eq. (7) is symmetrical with respect to μ and ν, here we consider only the μ component. Figure 2(a) corresponds to the μ component of Eq. (4), showing the relation between the original picture and high-order harmonics.

Figure 2(b) shows the decay characteristics of high-order harmonics for different aperture ratios, and Fig. 2(c) shows the spectrum of Eq. (7) for $\alpha/x_0 = 0.5$. In all figures, the values are normalized to become 1 when $\mu = 0$.

Figure 3 shows a two-dimensional representation of Fig. 2(c). According to Figs. 2 and 3, the picture quality factors of the flat display are described as follows.

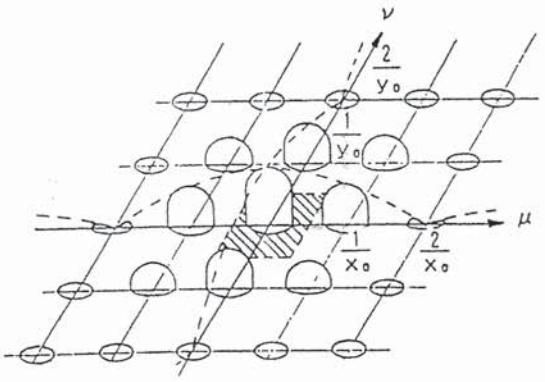

Fig. 3. Two-dimensional spatial frequency spectrum.

(1) Viewing distance and picture quality

As shown in Figs. 2(c) and 3, high-order harmonics are added to the original picture, leading to the sensation of roughness created typically by the flat display. Since these high-order harmonics can only be eliminated by the filtering effect of our vision, an appropriate viewing distance is necessary to achieve high picture quality.

(2) Pixel area (aperture ratio) and picture quality

If a constant luminance is assumed, the comparison of Figs. 2(a) and (c) reveals that there are two factors having opposite effects on the picture quality as the aperture ratio increases. The first factor is the decay of high-order harmonics which improves the picture quality by reducing the sensation of roughness and thereby the viewing distance [12]. The second factor is the reduction of the high-frequency component of the basic spectrum (of the original picture) at the decay ratio indicated by the shaded area in Fig. 2(c).

Generally speaking, the quality improvement due to the reduction in roughness is assumed to be more effective and, therefore, picture quality becomes better with an increase in aperture ratio. However, when the viewing distance is significantly large, i.e., when the high-order harmonics are eliminated by the filtering effect of our vision, it is possible that lower aperture ratios give better picture quality. Needless to say, however, that in designing any display, a high aperture ratio should be used to ensure a satisfactory luminance.

(3) Nyquist limits and picture quality

In the spatial frequency area, the high-order harmonics exist at the reciprocal lattice points [13] of the lattice arrangement of pixels. The maximum area where the basic spectrum and high-order harmonics are not overlapped is bounded by the Nyquist limits (shaded area in Fig. 3), which represent the limits of the spatial frequencies of the picture displayed. Since the Nyquist limits restrict the basic spectrum, their shape characterizes the picture. If the display area is the same, resolution improves as the area bounded by the Nyquist limits becomes larger.

3. Pixel Arrangement and Picture Quality in Color Displays

As is evident from the principle of the additive mixture of color stimuli, colors are expressed by vectors in a three-dimensional linear space. Therefore, Eq. (4) can be expressed by a vector consisting of the three primary color components:

$$\overrightarrow{Hs}(\mu,\nu)=\overrightarrow{Gs}(\mu,\nu)+\overrightarrow{Bs}(\mu,\nu)+\overrightarrow{Rs}(\mu,\nu) \qquad (8)$$

Figure 4 shows some typical pixel arrangements used for large-sized matrix displays. Let us call a light-emissive portion for a simple color a "dot" and the minimum unit containing the three primary colors a "pixel." Roughly speaking, in the RGB-trio, R, G, and B are integrated with the center of the pixel corresponding to the sampling of the picture. By contrast, in other arrangements (mosaic arrangements), R, G, and B are arranged separately, with the center of each dot corresponding to the sampling of the picture. In the following, a model of the color display is derived to elucidate how different pixel arrangements affect picture quality.

3.1. Color picture model

(1) Picture model for the RGB-trio

In the coordinate system shown in Fig. 4(a), the sampling of the picture can be obtained in the same manner for R, G, and B. The sampled picture is expressed by the following equations:

$$\overrightarrow{Gs}(\mu,\nu)=\frac{1}{3x_0y_0}\sum_k\sum_l\overrightarrow{G}\left(\mu-\frac{k}{\sqrt{3}x_0},\nu-\frac{l}{\sqrt{3}y_0}\right) \qquad (9a)$$

$$\overrightarrow{Bs}(\mu,\nu)=\frac{1}{3x_0y_0}\sum_k\sum_l\overrightarrow{B}\left(\mu-\frac{k}{\sqrt{3}x_0},\nu-\frac{l}{\sqrt{3}y_0}\right) \qquad (9b)$$

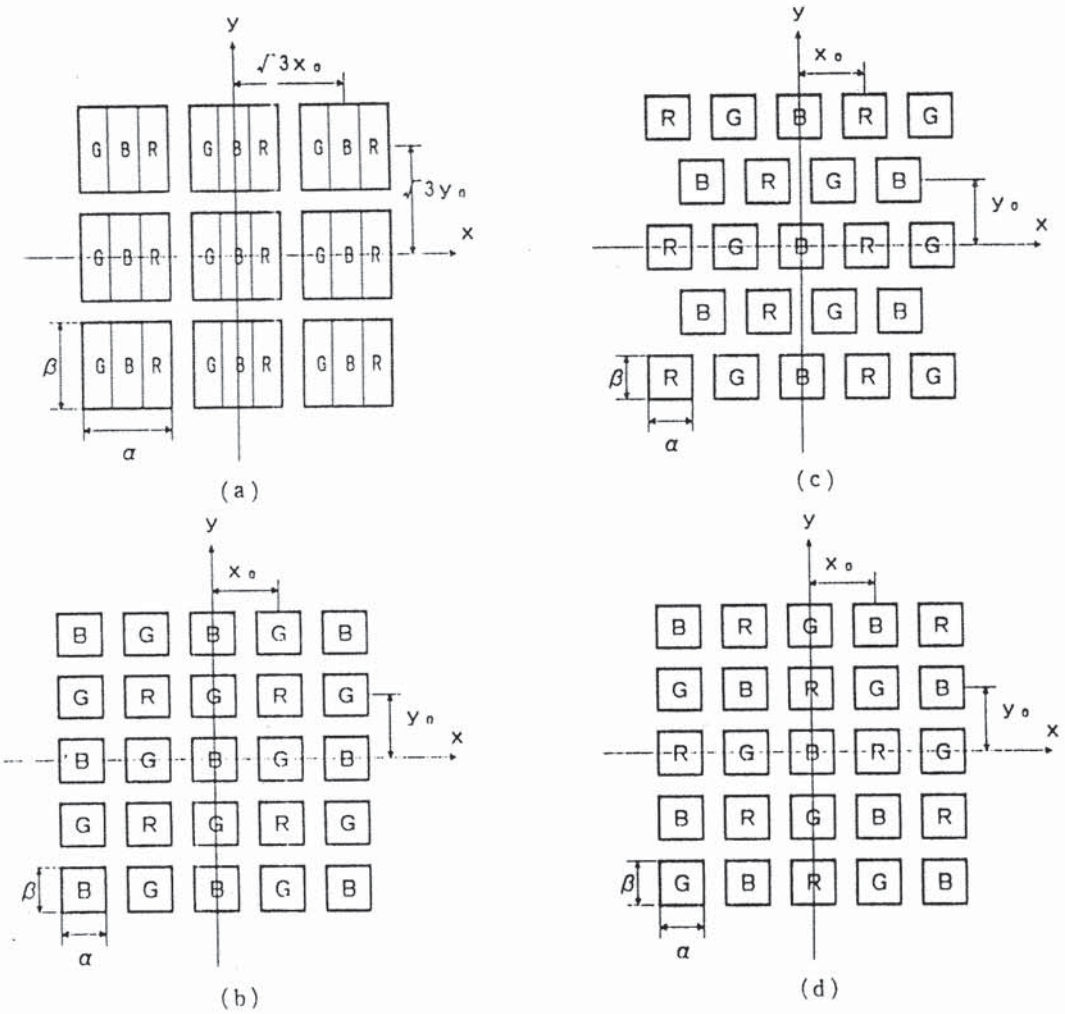

Fig. 4. (a) RGB-trio, (b) RGGB-mosaic, (c) RGB-delta, and (d) RGB-mosaic.

$$\overrightarrow{Rs}(\mu,\nu)=\frac{1}{3x_0y_0}\sum_k\sum_l\vec{R}\left(\mu-\frac{k}{\sqrt{3}x_0},\nu-\frac{l}{\sqrt{3}y_0}\right) \tag{9c}$$

By substituting Eqs. (9a), (9b), and (9c) into Eq. (8) and integrating according to Eq. (6), the picture model can be expressed by the equation shown below (Appendix 1). The range of integration of individual colors corresponds to the arrangement of dots. After being substituted into Eq. (8), Eqs. (9a), (9b), and (9c) are integrated assuming a uniform luminance within the dots. The interpretation of the model is provided in section 3.2:

$$\begin{aligned}\overrightarrow{Hd}(\mu,\nu)=&\int_{-\beta/2}^{\beta/2}\int_{-\alpha/2}^{\alpha/2}\overrightarrow{Hs}(\mu,\nu)\\&\cdot\exp(-2\pi\mu x)\cdot\exp(-2\pi\nu y)dxdy\\=&\frac{\alpha\beta}{3}\cdot\frac{\sin\pi\mu\alpha/3}{\pi\mu\alpha/3}\cdot\frac{\sin\pi\nu\beta}{\pi\nu\beta}\\&\cdot\{\overrightarrow{Gs}(\mu,\nu)\cdot\exp(2/3\pi j\mu\alpha)+\overrightarrow{Bs}(\mu,\nu)\\&+\overrightarrow{Rs}(\mu,\nu)\cdot\exp(-2/3\pi j\mu\alpha)\}\end{aligned} \tag{10}$$

(2) Picture model for mosaic arrangements

In the coordinate system shown in Figs. 4(b) to (d), sampling of the picture is obtained separately for R, G, and B. The sampled picture is expressed by the following equations (Appendix 2):

① RGGB-mosaic

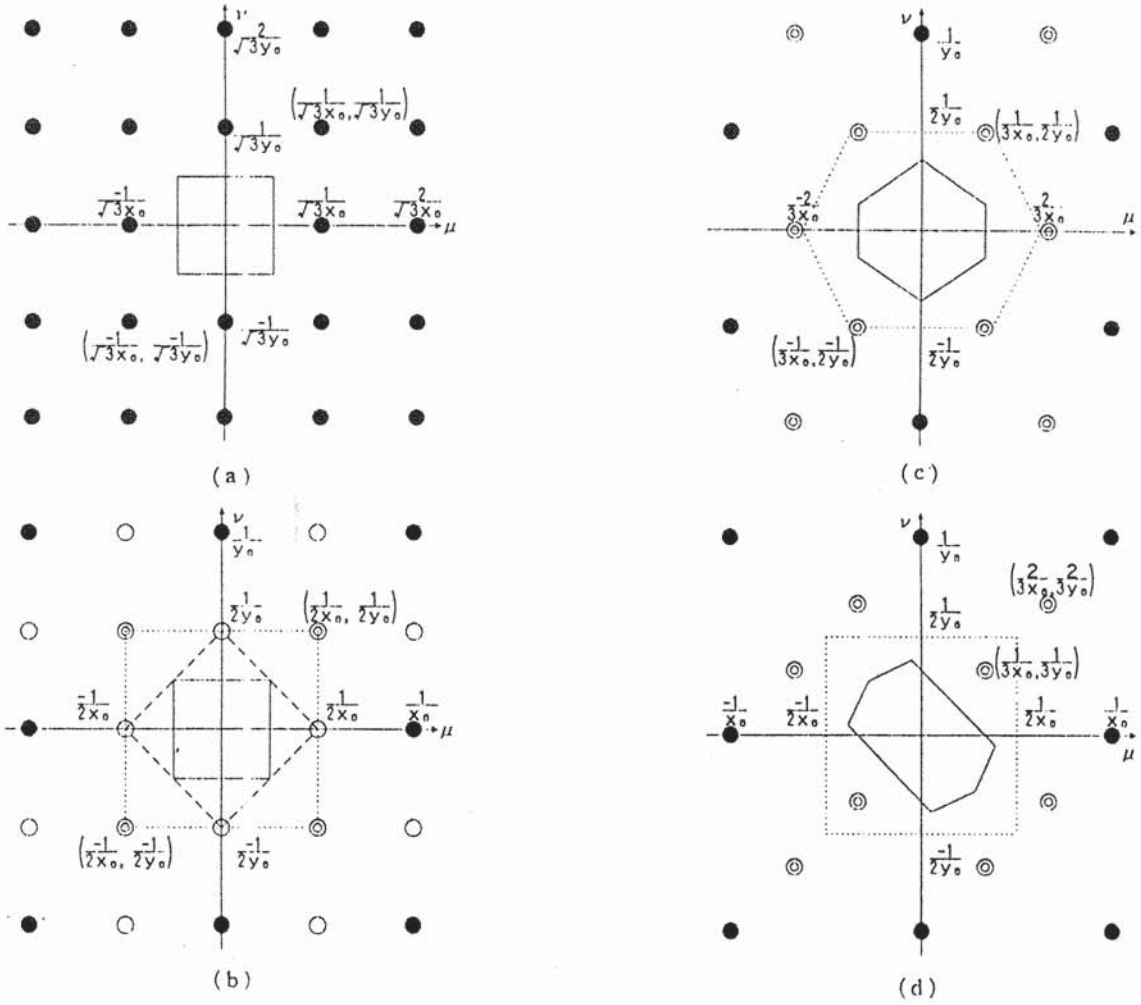

Fig. 5. (a) Nyquist limits of RGB-trio, (b) Nyquist limits of RGGB-mosaic, (c) Nyquist limits of RGB-delta, and (d) Nyquist limits of RGB-mosaic.

$$\vec{Gs}(\mu,\nu)=\frac{1}{4x_0y_0}\sum_k\sum_l\vec{G}\left(\mu-\frac{k}{2x_0},\nu-\frac{l}{2y_0}\right)\cdot\{(-1)^k+(-1)^l\} \tag{11a}$$

$$\vec{Bs}(\mu,\nu)=\frac{1}{4x_0y_0}\sum_k\sum_l\vec{B}\left(\mu-\frac{k}{2x_0},\nu-\frac{l}{2y_0}\right) \tag{11b}$$

$$\vec{Rs}(\mu,\nu)=\frac{1}{4x_0y_0}\sum_k\sum_l\vec{R}\left(\mu-\frac{k}{2x_0},\nu-\frac{l}{2y_0}\right)\cdot(-1)^{k+l} \tag{11c}$$

② RGB-delta

$$\vec{Gs}(\mu,\nu)=\frac{1}{6x_0y_0}\sum_k\sum_l\vec{G}\left(\mu-\frac{k}{3x_0},\nu-\frac{l}{2y_0}\right)\cdot\{1+(-1)^{k+l}\}\cdot\exp\left(\frac{2}{3}\pi jk\right) \tag{12a}$$

$$\vec{Bs}(\mu,\nu)=\frac{1}{6x_0y_0}\sum_k\sum_l\vec{B}\left(\mu-\frac{k}{3x_0},\nu-\frac{l}{2y_0}\right)\cdot\{1+(-1)^{k+l}\} \tag{12b}$$

$$\vec{Rs}(\mu,\nu)=\frac{1}{6x_0y_0}\sum_k\sum_l\vec{R}\left(\mu-\frac{k}{3x_0},\nu-\frac{l}{2y_0}\right)\cdot\{1+(-1)^{k+l}\}\cdot\exp\left(\frac{4}{3}\pi jk\right) \tag{12c}$$

③ RGB-mosaic

$$\overrightarrow{Gs}(\mu,\nu)=\frac{1}{9x_0y_0}\sum_k\sum_l\overrightarrow{G}\left(\mu-\frac{k}{3x_0},\nu-\frac{l}{3y_0}\right)\cdot\left\{1+\exp\frac{2}{3}\pi j(k-l)+\exp\frac{2}{3}\pi j(l-k)\right\}\cdot\exp\frac{2}{3}\pi jk \tag{13a}$$

$$\overrightarrow{Bs}(\mu,\nu)=\frac{1}{9x_0y_0}\sum_k\sum_l\overrightarrow{B}\left(\mu-\frac{k}{3x_0},\nu-\frac{l}{3y_0}\right)\cdot\left\{1+\exp\frac{2}{3}\pi j(k-l)+\exp\frac{2}{3}\pi j(l-k)\right\} \tag{13b}$$

$$\overrightarrow{Rs}(\mu,\nu)=\frac{1}{9x_0y_0}\sum_k\sum_l\overrightarrow{R}\left(\mu-\frac{k}{3x_0},\nu-\frac{l}{3y_0}\right)\cdot\left\{1+\exp\frac{2}{3}\pi j(k-l)+\exp\frac{2}{3}\pi j(l-k)\right\}\cdot\exp\frac{4}{3}\pi jk \tag{13c}$$

By substituting Eqs. (11) to (13) into Eq. (8) and integrating according to Eq. (6), all picture models for the aforementioned mosaic arrangements can be expressed by the following equation.

$$\begin{aligned}\overrightarrow{Hd}(\mu,\nu)&=\int_{-\alpha/2}^{\alpha/2}\int_{-\beta/2}^{\beta/2}\overrightarrow{Hs}(\mu,\nu)\cdot\exp(-2\pi\mu x)\cdot\exp(-2\pi\nu y)dxdy\\&=\alpha\beta\{\overrightarrow{Gs}(\mu,\nu)+\overrightarrow{Bs}(\mu,\nu)+\overrightarrow{Rs}(\mu,\nu)\}\cdot\frac{\sin\pi\mu\alpha}{\pi\mu\alpha}\cdot\frac{\sin\pi\nu\beta}{\pi\nu\beta}\end{aligned} \tag{14}$$

The interpretation of the models is provided in the following section.

3.2. Nyquist limits and visual limits

The picture quality provided by each pixel arrangement can be described on the basis of the interpretation of the corresponding picture model, i.e., Eq. (11) or (14). Basically, the picture quality is determined by the picture quality factors described in section 2.2. Since the viewing distance and aperture ratio are the same for all pixel arrangements, it follows that the Nyquist limits are the essential factor of the difference in picture quality. In the following discussion, the Nyquist limits of the aforementioned pixel arrangements are derived using the corresponding picture models to clarify their relation to human visual limits.

(1) Deriving Nyquist limits

As stated in section 2.2, in the spatial frequency region, the Nyquist limits bound the maximum area where the basic spectrum and high-order harmonics are not overlapped. Based on Eqs. (9) and (11) to (13), the relations between the basic spectra for individual pixel arrangements and their high-order harmonics are represented as shown in Figs. 5(a) to (d). In these figures, the black circle indicates that high-order harmonics for R, G, and B have the same sign and the double circle indicates that one of them has a different sign from the others. A single circle is unique to the RGGB-mosaic, indicating that no high-order harmonics for G exist there.

Nyquist limits can be obtained for each color, and the Nyquist limits common to all colors are called the colored region. A color picture is a sum of the vectors for R, G, and B spectra. In a mosaic arrangement having high-order harmonics with different signs, the common components (luminance components) of the high-order harmonics with different signs offset each other around the Nyquist limits of each color. This region is called the discolored region below.

In Figs. 5(a) to (d), the colored region is indicated by a solid line and the discolored region by a dotted line. In the RGGB-mosaic, although the Nyquist limits of G (dashed line) surrounds a large area, the colored region is determined by the Nyquist limits of B and R, which surrounds a smaller area.

(2) Nyquist limits and visual limit

From their definition, the Nyquist limits have to agree with our visual limit under appropriate viewing conditions. Chen et al. have evaluated what is called the colored region here and reported that this region is related to our visual limit by a coefficient similar to the Kell factor and that the Nyquist limits therefore do not agree with our visual limit [10]. However, the report does not provide the theoretical grounds for this argument. Here, the circular zone plate (CZP: Fig. 6) [14], expressed by the following equation and known as a means of evaluating the characteristics of displays, is used to establish the relation between the Nyquist limits and visual limit:

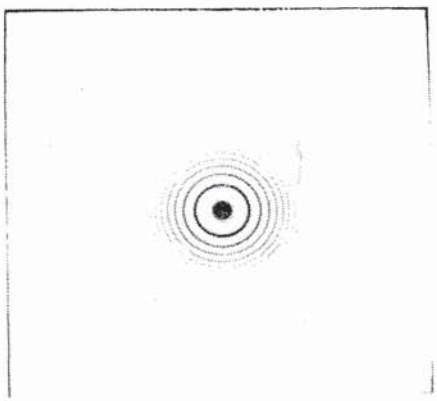

Fig. 6. Circular zone plate (CZP).

$$g(x, y)=\cos 2\pi\phi(x, y)=\cos\pi(x^2+y^2) \qquad (15)$$

The CZP satisfies the following relations; and, therefore, it allows us to observe the two-dimensional spatial frequency characteristics directly:

$$\mu=\partial\phi(x, y)/\partial x=x \qquad (16a)$$

$$\nu=\partial\phi(x, y)/\partial y=y \qquad (16b)$$

Figures 7(a) to (d) show the pictures of the original CZP having 512 × 480 pixels exhibited on displays based on different pixel arrangements. To ensure correspondence to Figs. 5(a) to (d), the RGB-trio has 128 × 120 pixels and the mosaic arrangements have 256 × 240 dots. Comparing Figs. 7(a) to (d) and Figs. 5(a) to (d) reveals that colored display is possible in the colored region. It is found also that in the discolored region, since the information is represented by one of the three primary colors, the shape of the original picture can be recognized despite discoloration. From these findings, it can be said that the Nyquist limits, as is required from their definition, agree with our visual limit. Therefore, it is possible to use them as the basis for discussing the characteristics of pixel arrangements.

3.3. Pixel arrangement and picture quality

(1) Comparison of RGB-trio and mosaic arrangements

The essential difference between the RGB-trio and mosaic arrangements is that the latter arrangements have the discolored region. The total areas surrounded by the Nyquist limits for R, G, and B are the same for both types of arrangements but mosaic arrangements provide higher resolution since they have discolored regions. In picture models, this is accounted for by the fact that the picture displayed by mosaic arrangements is sampled for each color dot and therefore includes more sampling points. At high spatial frequencies, visual sensitivity to colors decreases [15], diminishing the effect of discoloration. Therefore, the discolored region plays an important role in improving resolution.

(2) Comparison of different mosaic arrangements

There is no quantitative difference among mosaic arrangements which results in any difference in picture quality. They differ only in the manner in which R, G, and B are arranged; and it is their Nyquist limits that characterize picture quality.

① RGGB-mosaic

The RGGB-mosaic generally is regarded as providing high resolution because it contains a relatively large number of G dots to which human vision is more sensitive than to the other colors [1]. However, this arrangement is not necessarily rated highly in subjective evaluation tests [6]. This discrepancy is explained by taking into account the viewing distance.

When the viewing distance is small, the high-order harmonics of B and R, for which the RGGB-mosaic has fewer dots, make the picture look rough. This is a negative effect of the emphasis on G in the RGGB-mosaic. When the viewing distance is large, however, the high-order harmonics are eliminated by the filtering effect of our vision, thereby reducing the apparent sensation of roughness of the picture. Furthermore, the discoloration of fine lines does not seriously affect the picture quality since visual sensitivity to colors declines at high frequencies [15]. In this case, therefore, the emphasis on G leads to high resolution. It is considered that the evaluations using simulation pictures were conducted without taking into account the viewing distance and therefore under the conditions where the negative effect was more apparent.

② RGB-delta

This arrangement exhibits isotropic Nyquist limits and generally receives high ratings in subjective evaluation tests [6, 10]. The sampling of the RGB-delta is based on sub-Nyquist sampling [11]; and, therefore, it

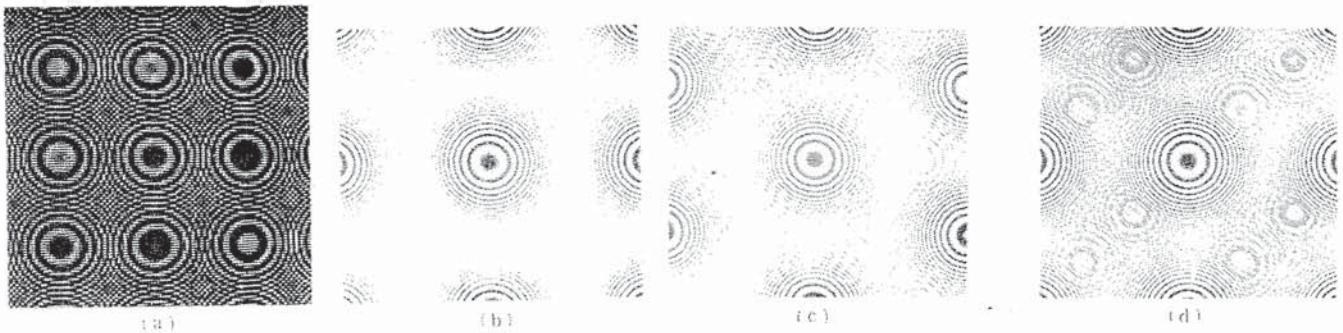

Fig. 7. Image of CZP for (a) RGB-trio, (b) RGGB-mosaic, (c) RGB-delta, and (d) RGB-mosaic.

Table 1. Specifications of simulation pictures

	RGGB-mosaic	RGB-trio	
	p_t / p_t	p_q / p_q	$(p_q/p_t)^2$
A	$p_t = 3$	$p_q = 4$	1.78
B	$p_t = 4$	$p_q = 6$	2.25
C	$p_t = 6$	$p_q = 8$	1.78
D	$p_t = 7$	$p_q = 10$	2.04
E	$p_t = 8$	$p_q = 12$	2.25

Pt ; Pixel pitch of RGB-trio
Pq ; Pixel pitch of RGGB-mosaic
Original Picture ; Carnation Girl(ITE test chart)
Note : Numerical value of a pixel pitch is the number of points of CRT of the simulator

inherently deteriorates the image of slant lines. Slant components generally are not regarded as crucial factors of picture quality [11]. However, the RGB-delta does not reproduce outlines as faithfully as the RGGB-mosaic [7]; and this is due partly to the poor quality of slant line images.

③ RGB-mosaic

The RGB-mosaic exhibits asymmetric Nyquist limits on the right and left sides, resulting in picture quality difference between slant lines in the northeast and northwest directions. This leads to slant line noise displayed over the entire screen, which is particularly conspicuous in matrix displays with a small number of dots.

4. Comparison of Picture Quality Provided by RGB-Trio and RGGB-Mosaic

Due to the structural constraints arising from the lattice arrangement of light-emissive elements, most large-sized matrix displays employ the RGB-trio or RGGB-mosaic. As is clarified in section 3, the essential factor differentiating these arrangements is the Nyquist limits and particularly the discolored region. Here, still and motion pictures provided by the RGB-trio and RGGB-mosaic are compared by means of subjective evaluation tests using still pictures and spectrum analysis of motion pictures to examine the properties of the discolored regions and thus compare the picture quality provided by both pixel arrangements.

4.1. Comparison of picture quality using a still picture

(1) Experiment

Five pairs of simulation pictures are created for the (1) RGB-trio and (2) RGGB-mosaic according to the specifications indicated in Table 1. All pictures are created by converting an original picture with 1024 × 1024 pixels into corresponding pixel specifications. In each pair, the RGB-trio has more pixels than the RGGB-mosaic, with the ratio of the number of pixels set

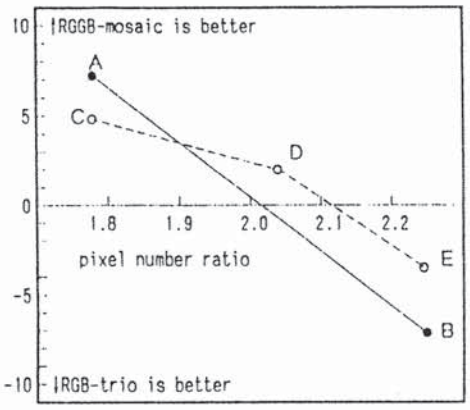

Fig. 8. Subjective evaluation results.

between 1.78 and 2.25. The experiment is conducted by showing the five pairs to subjects. Afterward, the subjects select one from among these evaluations: a) "(1) is better;" b) "(2) is better;" and (3) "I don't know." The evaluations a, b, and c are given ratings of -10, 10, and 0, respectively; and the results are averaged. The experiment involves 25 subjects who are not specialists in evaluating picture quality.

(2) Results

Figure 8 summarizes the results of the experiment. The horizontal axis represents the ratio of the number of pixels defined for A, B, C, D, and E in Table 1; and the vertical axis represents the average rating. The solid line shows the results obtained for a small pixel pitch and a long viewing distance, and the broken line shows those obtained for a large pixel pitch and a short viewing distance. The figure reveals that the RGB-trio provides a better picture quality when the ratio of the RGB-trio number of pixel to RGGB-mosaic is 2.25 times and that the RGGB-mosaic provides a better picture quality when the ratio is 1.78.

Therefore, both pixel arrangements provide much the same picture quality when the ratio is between 1.78 and 2.25, i.e., when the RGB-trio has about twice as many pixels as the RGGB-mosaic. The results indi- cated by the solid and broken lines show much the same trends, although those corresponding to the broken line exhibit larger variations depending on the subject.

4.2. Spectrum analysis of motion pictures

(1) Spectrum of pictures moving horizontally

When a picture moves horizontally (in the x direction) at a speed v, the picture at time t is expressed by the following equation:

$$h(x, y, t) = h(x - vt, y) \tag{17}$$

The two-dimensional Fourier transformation of this picture is expressed by

$$F\{h(x - vt, y)\} = H(\mu, \nu) \cdot \exp(-2\pi j \mu v t) \tag{18}$$

From Eqs. (7) and (18), the picture at time t on a display with a pixel area of $\alpha\beta$ is expressed by

$$\overrightarrow{Hd}(\mu, \nu, f) = \alpha\beta \frac{\sin\pi\mu\alpha}{\pi\mu\alpha} \cdot \frac{\sin\pi\nu\beta}{\pi\nu\beta} \overrightarrow{Hs}(\mu, \nu) \cdot \exp(-2\pi j \mu v t) \tag{19}$$

If the picture moves by one pixel or one dot at each field, Eq. (19) can be interpreted for the RGB-trio and RGGB-mosaic as follows. Interpretations for movement at any speed is provided later.

① RGB-trio (pixel pitch: $\sqrt{3}x_0$)

If we write $\mu = k/\sqrt{3}x_0$ from Eq. (9), when $v = \sqrt{3}x_0/t_0$ (t_0: field period) and time $t = nt_0$, $\exp(-2\pi j \mu v t)$ becomes 1. Therefore, the spectrum for the RGB-trio does not change due to the movement of the picture.

② RGGB-mosaic (dot pitch: x_0)

If we write $\mu = k/(2x_0)$ from Eqs. (11), when $v = x_0/t_0$ and time $t = nt_0$, Eq. (19) becomes as follows. Therefore, in the spectrum for the RGGB-mosaic, the odd-number-th order harmonics in the direction of the movement reverses their signs at each field:

$$\overrightarrow{Hd}(\mu, \nu, f) = \alpha\beta \frac{\sin\pi\mu\alpha}{\pi\mu\alpha} \cdot \frac{\sin\pi\nu\beta}{\pi\nu\beta} \cdot \overrightarrow{Hs}(\mu, \nu) \cdot (-1)^{nk} \tag{20}$$

(2) Spectrum of motion picture and visual limit

The TFZP (to-and-fro zone plate) method [14, 16] is used to examine how the reversing of the signs of high-order harmonics at each field appear on the real display.

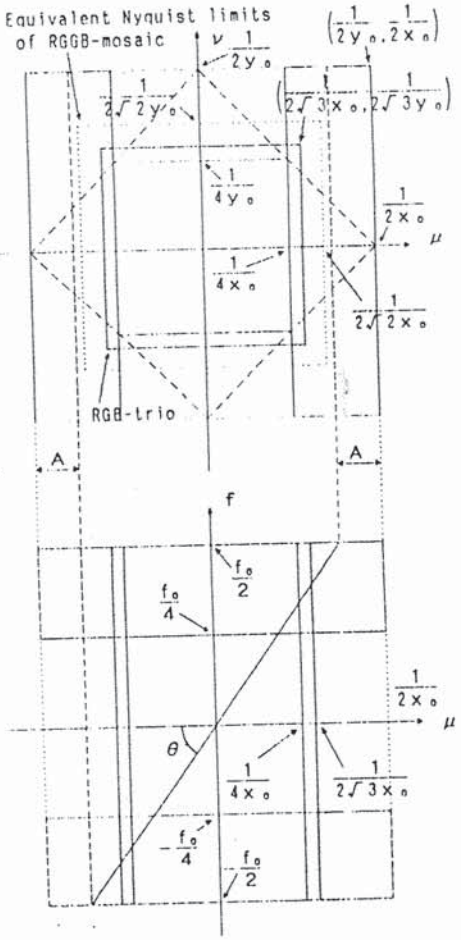

Fig. 9. The spectrum of the moving picture.

Express a CZP moving in the horizontal direction at speed v by the following equation:

$$g(x, y, t)=\cos 2\pi\phi(x, y, t)=\cos\pi\{(x+vt)^2+y^2\} \tag{21}$$

From Eq. (21), we have the following relations:

$$\mu=\partial\phi(x, y, t)/\partial x=x, \tag{22a}$$

$$\nu=\partial\phi(x, y, t)/\partial y=y, \tag{22b}$$

$$f=\partial\phi(x, y, t)/\partial t\,|_{t=0}=v\mu \tag{22c}$$

If the movement of the picture is considered, the Nyquist limits obtained in the previous section can be represented as a three-dimensional structure shown in Fig. 9. The RGB-trio and RGGB-mosaic are shown in the same coordinate system to facilitate comparison. In

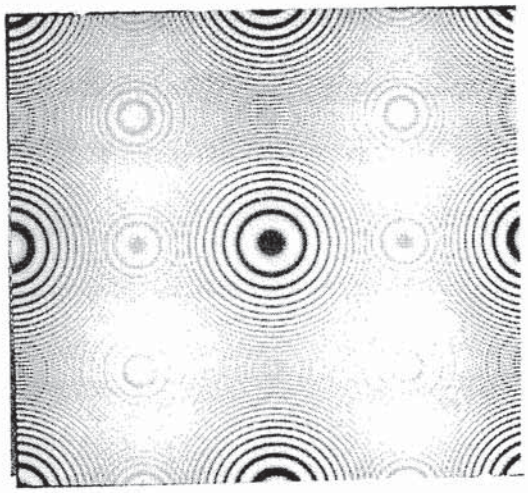

Fig. 10. Image of TFZP (to-and-fro zone plate) for RGGB-mosaic.

the figure, f_0 is the field frequency and the plane where $f = 0$ corresponds to the two-dimensional Nyquist limits. The shaded part indicates the area where, at a speed of $v = x_0/t_0$, the signs of high-order harmonics for the RGGB-mosaic are reversed at each field.

The spectrum of a picture moving at a speed of v ($=f/\mu = \tan\theta$) is represented by the plane which forms angle θ with the μ-v plane. As shown by portion A in Fig. 9, it becomes impossible to display high-frequency components as the speed increases. The TFZP method makes it possible to observe directly the spectrum on this plane.

Figure 10 shows the picture of TFZPs for $v = x_0/t_0$, i.e., two kinds of CZPs, one shifted by one dot from the other, and which alternately appear at each field displayed by the RGGB-mosaic. The area corresponding to the shaded portion in Fig. 9 appears to be the same as the colored region. Specifically, in the area surrounded by the Nyquist limits of the RGGB-mosaic, the high-order harmonics with opposite signs accumulate with time which changes the discolored region to a colored region.

4.3. Discussion

(1) Characteristics of the discolored region in the display of a still picture

The number of pixels represents the amount of information included in the picture. The greater the

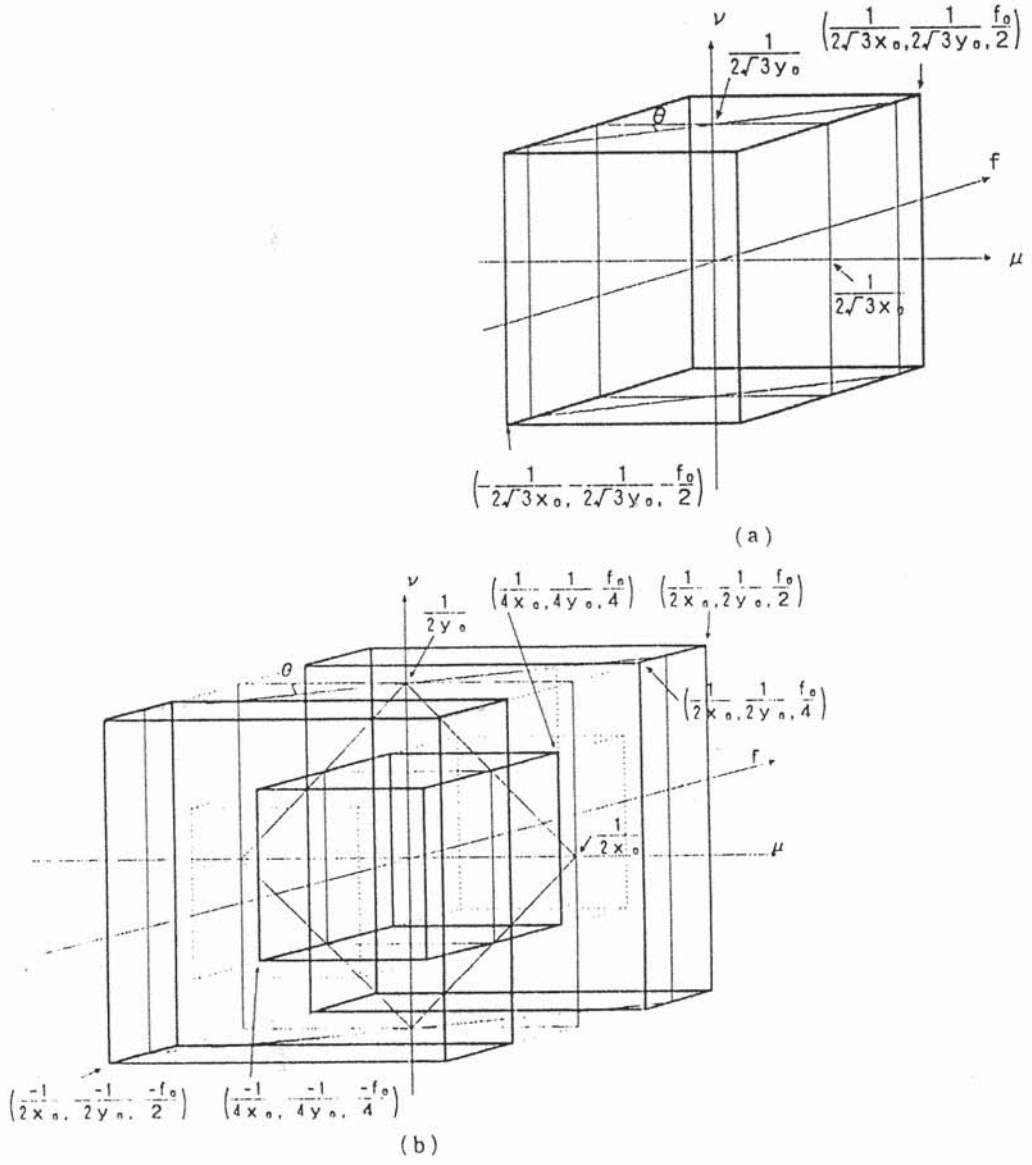

Fig. 11. (a) Three-dimensional Nyquist limits of (a) the RGB-trio and (b) the RGGB-mosaic.

number of pixels, the better the picture quality. By assuming that pictures with the same quality have the same number of pixels, the number of pixels, which is an objective quantity, can be related to picture quality, which is a subjective quantity. If the term "the number of pixels" is used in this sense (effective number of pixels), the experimental results shown in section 4.1 indicate that the RGGB-mosaic has an effective number of pixels almost twice the number of real pixels. The discolored region of the RGGB-mosaic contributes to this double increase in the number of pixels.

This increase is due to the overlap of adjacent pixels. The RGB-trio does not have this overlapping and thus no discolored region. The equivalent Nyquist limits shown in Fig. 9 are obtained from the effective, i.e., equivalent, number of pixels of the RGGB-mosaic. The picture quality of still pictures provided by the RGB-trio and RGGB-mosaic can be compared in terms of the equivalent number of pixels or equivalent Nyquist limits.

(2) Characteristics of the discolored region in the display of motion pictures

When the picture moves in the horizontal direction, the RGB-trio does not change the spectrum of the picture, while the RGGB-mosaic reverses the signs of high-order harmonics, thus changing the discolored region to

a colored region. The same occurs when the picture moves in the vertical direction.

This relation between the spectrum and Nyquist limits can be represented in three-dimensional space (three-dimensional Nyquist limits in Fig. 11). Figure 11(a) shows the three-dimensional Nyquist limits of the RGB-trio, and Fig. 11(b) shows those of the RGGB-mosaic. The area surrounded by bold lines represent the colored regions. As in Fig. 9, the plane where $f = 0$ corresponds to the two-dimensional Nyquist limits and the spectrum of a picture moving in the horizontal direction at speed v is shown on the plane forming angle θ with the μ-v plane. The figures reveal that, when the picture moves, the RGGB-mosaic expands the colored region, providing a better picture quality than for still pictures.

5. Conclusions

Using a model of the flat display incorporating picture sampling, it has been shown that the picture quality is determined by the viewing distance, pixel aperture ratio, and Nyquist limits. At the same time, it has been established that the Nyquist limits are the essential factor which produces the difference in picture quality among different pixel arrangements.

In mosaic arrangements, it has been found that the area surrounding by Nyquist limits consists of the colored and discolored regions. Based on this result, the Nyquist limits were related to our visual limit and to picture quality. In addition, the picture quality provided by two typical pixel arrangements, the RGB-trio and RGGB-mosaic, were compared. Experiments have revealed that, because of its discolored region, the RGGB-mosaic has an equivalent number of pixels, almost twice as large as its real number of pixels.

A spectrum analysis of motion pictures was performed to obtain the structures of three-dimensional Nyquist limits. It has been clarified theoretically that, in the RGGB-mosaic, the picture quality of motion pictures is improved over that of still pictures. This has been established through an experiment using the TFZP method.

In conclusion, the RGGB-mosaic increases the effective number of pixels when displaying still pictures and it further improves the picture quality when displaying motion pictures. Therefore, the RGGB-mosaic is an efficient pixel arrangement for applications such as sports stadiums which involve sufficient viewing distances and motion pictures. By employing the RGGB-mosaic, it is possible to provide high picture quality with a small number of dots.

No established criteria are available as yet for comparing the resolution of the RGB-trio and RGGB-mosaic. The number of pixels employed occasionally for this purpose is disadvantageous for the RGGB-mosaic. The existence and behavior of the discolored region established here may provide a practical means for evaluating resolution in the design of not only large-sized matrix displays but other types of flat displays as well. We intend to extend our study further to general pixel arrangements for a more comprehensive theoretical elucidation of the quality of motion pictures.

Acknowledgement. The authors wish to express their thanks to Mr. Haraguchi, Manager of Image and Information Systems Department, Nagasaki Works, Mitsubishi Electric Corporation, for his advice and instructions in completing this paper. Thanks are also due to all those who cooperated with the authors in carrying out experiments.

REFERENCES

1. K. Kurahashi, K. Yanagishita, H. Kobayashi, E. Okubo, and N. Tomimatsu. Aurora Vision—Large-screen color display system. ITEJ Technical Report, **IPD-49-3**, pp. 31-36 (1980).
2. K. Kurahashi. Giant screen display using an array of light-emitting devices. Jour. ITEJ, **38**, 1, pp. 21-25 (1984).
3. T. Hase, Z. Hara, S. Iwata, M. Masuda, and K. Tatsuda. The large-scale display "Diamond Vision Mark II" and its new drive method. Jour. ITEJ, **42**, 10, pp. 1112-1119 (1988).
4. Z. Hara, K. Shibayama, S. Iwata, K. Tatsuda, K. Seko, H. Kamogawa, S. Uemura, T. Shimojo, and Y. Kani. A lighting element for high-resolution, large-screen video display. ITEJ Technical Report, **IPD-91-87**, pp. 15-20 (1991).
5. M. Hayashi, T. Muchi, and M. Ozaki. A 15-mm trio pitch Jumbotron device. SID '89 Digest, pp. 98-101 (1989).
6. S. Tsuruta, K. Mitsuhashi, S. Ichikawa, and K. Noguchi. Color pixel arrangement evaluation for LC-TV. IDRC '85, pp. 24-26 (1985).

7. H. Nakamura, Y. Namikoshi, E. Shiohama, and Y. Tabuchi. Visual requirements of large-scale color display system. Proc. IEIJ 1989 National Convention, 81 (1989).
8. L. D. Silverstein, R. W. Monty, F. E. Gomer, and Y. Y. Yeh. A psychophysical evaluation of pixel mosaics and gray-scale requirements for color matrix displays. SID '89 Digest, pp. 128-131 (1989).
9. F. Inoue, K. Ando, N. Kabuto, M. Kamiya, R. Nashimoto, K. Suzuki, H. Suzuki, T. Tsukada, H. Kawakami, and M. Nakatani. A 5-inch diagonal liquid-crystal color TV. Proc. SID, **29**, 4, pp. 265-273 (1988).
10. L. Chen and S. Hasegawa. Two-dimensional visual resolution limits for matrix devices. Jour. ITEJ, **46**, 5, pp. 615-623 (1992).
11. T. Fukinuki. Digital Signal Processing of Image, pp. 62-72. Nikkan Kogyo Shimbun, Inc. (1984).
12. T. Hase, N. Shiramatsu, and S. Tomita. Effects of mosaic pixel structure on display images. Jour. ITEJ, **47**, 3, pp. 356-363 (1993).
13. O. Yoshida, and A. Iwamoto. Two-dimensional Nyquist limit and MTF for solid-state image sensor. Jour. ITEJ, **37**, 10, pp. 819-825 (1983).
14. T. Fukinuki. Multidimensional Processing of TV Signal, pp. 17-28. Nikkan Kogyo Shimbun, Inc. (1988).
15. H. Sakata and H. Isono. Chromatic spatial frequency characteristics of human visual system (color difference discrimination). Jour. ITE, **31**, 1, pp. 29-34 (1977).
16. T. Fukinuki and Y. Hirano. The To-and-Fro Zone Plate (TFZP) method for observing frequency characteristics in three dimensions. SMPTE J. Sept. '86, pp. 899-902 (1986).

APPENDIX

1. Derivation of Eq. (10)

$$\begin{aligned}\overrightarrow{Hd}(\mu,\nu)&=\int_{-\beta/2}^{\beta/2}\int_{-\alpha/2}^{\alpha/2}\overrightarrow{Hs}(\mu,\nu)\\&\quad\cdot\exp(-2\pi\mu x)\cdot\exp(-2\pi\nu y)dxdy\\&=\overrightarrow{Gs}(\mu,\nu)\int_{-\beta/2}^{\beta/2}\int_{-\alpha/3}^{-\alpha/6}\exp(-2\pi\mu x)\\&\quad\cdot\exp(-2\pi\nu y)dxdy\\&\quad+\overrightarrow{Bs}(\mu,\nu)\int_{-\beta/2}^{\beta/2}\int_{-\alpha/6}^{\alpha/6}\exp(-2\pi\mu x)\\&\quad\cdot\exp(-2\pi\nu y)dxdy\\&\quad+\overrightarrow{Rs}(\mu,\nu)\int_{-\beta/2}^{\beta/2}\int_{\alpha/6}^{\alpha/3}\exp(-2\pi\mu x)\\&\quad\cdot\exp(-2\pi\nu y)dxdy\\&=\frac{\alpha\beta}{3}\cdot\frac{\sin\pi\mu\alpha/3}{\pi\mu\alpha/3}\cdot\frac{\sin\pi\nu\beta}{\pi\nu\beta}\\&\quad\cdot\{\overrightarrow{Gs}(\mu,\nu)\cdot\exp(2/3\pi j\mu\alpha)\\&\quad+\overrightarrow{Bs}(\mu,\nu)+\overrightarrow{Rs}(\mu,\nu)\cdot\exp(-2/3\pi j\mu\alpha)\}\end{aligned}\tag{10}$$

2. Derivation of Eqs. (11) to (13)

The spectrum of the sampled picture can be obtained from the Fourier transformation of the sampling function as follows (* indicates convolution). Thus, the Fourier transformations of individual sampling functions are calculated to derive Eqs. (11) to (13):

$$\begin{aligned}Hs(\mu,\nu)&=H(\mu,\nu)*\frac{1}{x_0y_0}\sum_k\sum_l\delta\left(\mu-\frac{k}{x_0},\nu-\frac{l}{y_0}\right)\\&=\frac{1}{x_0y_0}\sum_k\sum_l H\left(\mu-\frac{k}{x_0},\nu-\frac{l}{y_0}\right)\end{aligned}$$

① RGGB-mosaic

The sampling function for B and its Fourier transformation are

$$\begin{aligned}sb(x,y)&=\sum_m\sum_n\delta(x-2mx_0,y-2ny_0)\\Sb&=\frac{1}{4x_0y_0}\sum_k\sum_l\delta\left(\mu-\frac{k}{2x_0},\nu-\frac{l}{2y_0}\right)\end{aligned}\tag{A1}$$

The Fourier transformation of the sampling function for G is the sum of the two functions obtained by shifting Eq. (A1) by $(x_0, 0)$ and $(0, y_0)$:

$$Sg=Sb\cdot\exp(-2\pi j\mu x_0)+Sb\cdot\exp(-2\pi j\nu y_0)$$

If we write $\mu = k/2x_0$ and $\nu = 1/2y_0$, then

$$Sg=\frac{1}{4x_0y_0}\sum_k\sum_l\delta\left(\mu-\frac{k}{2x_0},\nu-\frac{l}{2y_0}\right)\cdot\{(-1)^k+(-1)^l\} \quad \text{(A2)}$$

The Fourier transformation of the sampling function for R is obtained by shifting Eq. (A1) by (x_0, y_0). Thus,

$$Sr=Sb\cdot\exp(-2\pi j\mu x_0)\exp(-2\pi j\nu y_0)$$

If we write $\mu = k/2x_0$ and $\nu = 1/2y_0$, then

$$Sr=\frac{1}{4x_0y_0}\sum_k\sum_l\delta\left(\mu-\frac{k}{2x_0},\nu-\frac{l}{2y_0}\right)(-1)^{k+l} \quad \text{(A3)}$$

Using Eqs. (A1) to (A3), we arrive at Eqs. (11a) to (11c).

② RGB-delta

The sampling function for B (sum of two lattice sampling functions) and its Fourier transformation are

$$sb=\sum_m\sum_n\delta(x-3mx_0,y-2ny_0)+\sum_m\sum_n\delta\left(x-3mx_0-\frac{3}{2}x_0,y-2ny_0-y_0\right)$$

$$Sb=\frac{1}{6x_0y_0}\sum_k\sum_l\delta\left(\mu-\frac{k}{3x_0},\nu-\frac{l}{2y_0}\right)\cdot\left\{1+\exp\left(-2\pi j\mu\frac{3}{2}x_0\right)\exp(-2\pi j\nu y_0)\right\}$$

If we write $\mu = k/3x_0$ and $\nu = l/2y_0$, then

$$Sb=\frac{1}{6x_0y_0}\sum_k\sum_l\delta\left(\mu-\frac{k}{3x_0},\nu-\frac{l}{2y_0}\right)\{1+(-1)^{k+l}\} \quad \text{(A4)}$$

The Fourier transformation of the sampling function for G is obtained by shifting Eq. (A4) by $(-x_0, 0)$. Thus,

$$Sg=Bs\cdot\exp(2\pi j\mu x_0)$$

If we write $\mu = k/3x_0$, then

$$Sg=\frac{1}{6x_0y_0}\sum_k\sum_l\delta\left(\mu-\frac{k}{3x_0},\nu-\frac{l}{2y_0}\right)\cdot\{1+(-1)^{k+l}\}\cdot\exp\left(\frac{2}{3}\pi jk\right) \quad \text{(A5)}$$

The Fourier transformation of the sampling function for R is obtained by shifting Eq. (A5) by $(-x_0, 0)$. Thus,

$$Sr=Sg\cdot\exp(2\pi j\mu x_0)$$

If we write $\mu = k/3x_0$, then we have

$$Sr=\frac{1}{6x_0y_0}\sum_k\sum_l\delta\left(\mu-\frac{k}{3x_0},\nu-\frac{l}{2y_0}\right)\cdot\{1+(-1)^{k+l}\}\cdot\exp\left(\frac{4}{3}\pi jk\right) \quad \text{(A6)}$$

Using Eqs. (A4) to (A6), we arrive at Eqs. (12a) to (12c).

③ RGB-mosaic

The sampling function for B (sum of three lattice sampling functions) and its Fourier transformation are

$$sb(x,y)=\sum_m\sum_n\delta(x-3mx_0,y-3ny_0)+\sum_m\sum_n\delta(x-3mx_0-x_0,y-3ny_0-2y_0)+\sum_m\sum_n\delta(x-3mx_0-2x_0,y-3ny_0-y_0)$$

$$Sb=\frac{1}{9x_0y_0}\sum_k\sum_l\delta\left(\mu-\frac{k}{3x_0},\nu-\frac{l}{3y_0}\right)\cdot\{1+\exp(-2\pi j\mu x_0)\cdot\exp(-2\pi j\nu 2y_0)+\exp(-2\pi j\mu 2x_0)\cdot\exp(-2\pi j\nu y_0)\}$$

If we write $\mu = k/3x_0$ and $\nu = 1/3y_0$, then

$$Sb=\frac{1}{9x_0y_0}\sum_k\sum_l\delta\left(\mu-\frac{k}{3x_0},\nu-\frac{l}{3y_0}\right)\cdot\left\{1+\exp\frac{2}{3}\pi j(l-k)+\exp\frac{2}{3}\pi j(k-l)\right\} \quad \text{(A7)}$$

The Fourier transformation of the sampling function for G is obtained by shifting Eq. (A7) by $(-x_0, 0)$. Thus,

$$Sg=Sb\cdot\exp(2\pi j\mu x_0)$$

If we write $\nu = k/3x_0$, then

$$Sg=\frac{1}{9x_0y_0}\sum_k\sum_l\delta\left(\mu-\frac{k}{3x_0},\nu-\frac{l}{3y_0}\right)$$

$$\cdot\left\{1+\exp\frac{2}{3}\pi j(l-k)+\exp\frac{2}{3}\pi j(k-l)\right\}\exp\frac{2}{3}\pi jk \tag{A8}$$

The Fourier transformation of the sampling function for R is obtained by shifting Eq. (A8) by $(-x_0, 0)$. Thus,

$$Sr = Sg\cdot\exp(2\pi j\mu x_0)$$

If we write $\mu = k/3x_0$, then we have

$$\frac{1}{9x_0y_0}\sum_k\sum_l\delta\left(\mu-\frac{k}{3x_0},\nu-\frac{l}{3y_0}\right)\cdot\left\{1+\exp\frac{2}{3}\pi j(l-k)+\exp\frac{2}{3}\pi j(k-l)\right\}\exp\frac{4}{3}\pi jk \tag{A9}$$

Using Eqs. (A7) to (A9), we arrive at Eqs. (13a) to (13c).

AUTHORS (from left to right)




Zen-ichiro Hara received his M.S. degree in Electrical Engineering from Kyushu University, Japan, in 1981. In 1981, he joined Mitsubishi Electric Corporation. He has been engaged in the research and development of large-sized matrix displays. He is now a chief engineer in the Image and Information Systems Department of Nagasaki Works. He is a member of the Institute of Television Engineers of Japan.

Nobuo Terazaki received his B.S. degree in Electronic Engineering from Kogakuin University, Japan, in 1972 and joined Mitsubishi Electric Corporation. He has been engaged in the development of advanced systems of microprocessors and information display systems. He is now a manager of information display systems in Image and Information Systems Department of Nagasaki Works.

Naoki Shiramatsu received his M.S. degree in Biophysical Engineering from Osaka University, Japan, in 1987 and joined Mitsubishi Electric Corporation. He has been engaged in the development of color emissive displays and research on analysis of picture quality. He is now a research member in the Materials and Electronic Devices Laboratory. He is a member of the Institute of Electronics, Information, and Communication Engineers and the Institute of Television Engineers of Japan.

Shuji Iwata joined the Central Research Laboratory of Mitsubishi Electric Corporation in 1968. He has been engaged in the research and development of facsimile systems and information display systems. He is now a Research Manager of the CRT development group in the Materials and Electronic Devices Laboratory. He received Best Paper Awards from the Consumer Electronics Society of IEEE in 1987. He is a member of the Society for Information Display; the Institute of Electronics, Information, and Communication Engineers; and the Institute of Television Engineers of Japan.